JOURNAL OF BONE AND MINERAL RESEARCH
Volume 24, Number 5, 2009
Published online on December 29, 2008; doi: 10.1359/JBMR.081239

Atp6v0d2 Is an Essential Component of the Osteoclast-Specific Proton Pump That Mediates Extracellular Acidification in Bone Resorption

Haiping Wu,[1,2] Guoliang Xu,[2] and Yi-Ping Li[3,4]

ABSTRACT: Bone resorption relies on the extracellular acidification function of vacuolar (V-) ATPase proton pump(s) present in the plasma membrane of osteoclasts. The exact configuration of osteoclast-specific V-ATPases remains largely unknown. In this study, we found that Atp6v0d2 (d2), an isoform of the d subunit in the V-ATPase, showed 5-fold higher expression than that of Atp6v0d1 (d1) in mature osteoclasts, indicating a potential function in osteoclastic bone resorption. When d2 was depleted at an early stage of RANKL-induced osteoclast differentiation in vitro, formation of multinucleated cells was severely impaired. However, depletion of d2 at a late differentiation stage did not affect osteoclast fusion but did abolish the activity of extracellular acidification and bone resorption of mature osteoclasts. We also showed the association of the two tagged-proteins d2 and a3 when co-expressed in mammalian cells with a co-immunoprecipitation assay. Moreover, glutathione-*S*-transferase (GST) pull-down assay showed the direct interaction of d2 with the N terminus of Atp6v0a3 (a3), which is the functionally identified osteoclast-specific component of V-ATPase. Therefore, our results show the dual function of d2 as a regulator of cell fusion in osteoclast differentiation and as an essential component of the osteoclast-specific proton pump that mediates extracellular acidification in bone resorption.
J Bone Miner Res 2009;24:871–885. Published online on December 29, 2008; doi: 10.1359/JBMR.081239

Key words: Atp6v0d2, vacuolar-ATPases, osteoclasts, bone resorption, extracellular acidification

Address correspondence to: *Yi-Ping Li, PhD, Department of Cytokine Biology, the Forsyth Institute, 140 the Fenway, Boston, MA 02115, USA, E-mail: ypli@forsyth.org*

INTRODUCTION

Bone homeostasis is dynamically maintained by both the bone degradation of osteoclasts and bone formation of osteoblasts.[1–3] Many diseases, such as osteoporosis, rheumatoid arthritis, and osteopetrosis, are mostly or partially caused by abnormal activities of osteoclasts.[4–6] The osteoclasts capable of resorption are giant multinucleated cells (MNCs) derived from monocyte/macrophage lineage precursor cells that become ultimately mature by fusion from mononuclear pre-osteoclasts.[2,3,7] Bone resorption is ascribed to extracellular acidification in the ruffled border. A resorption lacuna beneath a mature osteoclast is where the low pH microenvironment contributes to resorption of the bone matrix, including the degradation of inorganic minerals and the enzymatic hydrolysis of the organic components.[1,3,8] It has been widely accepted that the cellular acidification depends on the ATP-driven proton pump, the vacuolar type H^+-ATPase (V-ATPase) complex ubiquitously distributed in the membrane of such intracellular organelles as clathrin-coated vesicles, endosomes, the Golgi complex, and lysosomes, as well as in the plasma membrane of certain cell types, including renal intercalated cells and osteoclasts.[9–12] Conserved in eukaryotes from yeast to mammalian cells, this proton pump is a multi-subunit complex composed of two domains that allow for coupling to form an integrated active V-ATPase: a peripheral V_1 domain involved in ATP hydrolysis and a membrane integral V_0 domain with a function of proton transport.[10,11,13] In mammalian cells, a widely accepted structural model for the composition of this bidomain complex has been depicted in which eight different subunits (A–H) compose V_1, and five subunits (a, c, c″, d, and e) associate to form V_0 and to hold V_1 at the membrane.[10,11,14]

Multiple isoforms of some subunits in V-ATPase, including B, C, E, and G of V_1 and a and d of V_0, have been identified in various tissues and cell types, where diverse functions for these isoforms are needed.[15–18] For example, four isoforms have been characterized for subunit a.

The authors state that they have no conflicts of interest.

[1]State Key Laboratory of Molecular Biology, Institute of Biochemistry and Cell Biology, Shanghai Institutes for Biological Sciences, Chinese Academy of Sciences, Shanghai, China; [2]Graduate School of Chinese Academy of Sciences, Shanghai, China; [3]Department of Cytokine Biology, the Forsyth Institute, Boston, Massachusetts, USA; [4]Department of Developmental Biology, Harvard School of Dental Medicine, Boston, Massachusetts, USA.

We previously reported that one of the a subunit isoforms, Atp6v0a3 (a3, also known as Atp6i or Tcirg1), is prominently expressed in osteoclasts[19,20] and that *Atp6i* disruption in mice resulted in severe osteopetrosis phenotype because of the loss of extracellular acidification.[21] Mutational analysis in patients with infantile malignant autosomal recessive osteopetrosis (MIM259700) indicated that lack of a functional a3 subunit causes severe osteopetrosis because of impairment of bone resorption.[21,22] Recently, another osteoclast-specific proton pump subunit Atp6v1C1 (C1) was also reported to be involved in the formation of filamentous (F-) actin rings in osteoclasts.[23] Previous reports have provided evidence that V-ATPase complexes may selectively form to contain particular combinations of subunit isoforms in certain cell types.[17,24] Therefore, it remains assumed, but not proven, that a distinct V-ATPase complex serving in extracellular acidification exists in the plasma membrane of osteoclasts, combined with certain subunits (e.g., a3 or C1) required for the function of bone resorption by osteoclasts.

A 38-kDa protein Atp6v0d2 (d2), one of the two closely related isoforms for subunit d, has been found to be expressed in various mammalian tissues and is the most abundant in osteoclasts.[15–17,25–28] It shows a much more specific expression profile than the other isoform Atp6v0d1 (d1), suggesting a different role(s) in certain cell types.[26] Studies of the homolog of subunit d in yeast *Saccharomyces cerevisiae* suggested that this subunit may contribute to the efficient coupling of ATP hydrolysis of V_1 and proton translocating of V_0.[15] A recent gene targeting study has reported that *Atp6v0d2*$^{-/-}$ mice showed osteopetrosis phenotype. This osteopetrosis phenotype was attributed to the failure of pre-osteoclast fusion into mature multinucleated cells.[29] However, other roles of d2 in V-ATPase activity (beyond cell fusion) could not be ruled out because the possibility of studying d2 function in normal mature osteoclasts was precluded by the impaired formation of mature osteoclasts induced with RANKL from *Atp6v0d2*$^{-/-}$ bone marrow–derived macrophages (BMMs) in vitro.[29] Therefore, the functional importance of d2 in the osteoclast proton pump still needs to be further established.

In this study, we characterized d2 in our search for osteoclast-specific pump subunits using microarray analysis in human mature osteoclasts as described[30–32] and confirmed its upregulation in osteoclast differentiation in vitro.[29] We performed lentivirus-mediated RNA interference (RNAi) knockdown of d2 expression in vitro at different osteoclast differentiation stages.[32] Consistently with the mouse model, depletion of d2 at an early differentiation stage impaired pre-osteoclast fusion.[29] However, the knockdown of d2 expression at a late differentiation stage did not affect maturation of osteoclasts but impaired the multinucleated cell functions of bone resorption and extracellular acidification. We also validated the association of d2 and a3 by glutathione-*S*-transferase (GST) pull-down and co-immunoprecipitation (co-IP) assays. Our results suggest that Atp6v0d2 has dual functions in osteoclasts both for regulation of osteoclast maturation and for extracellular acidification when it serves as a component of V-ATPase in mature osteoclasts.

MATERIALS AND METHODS

Constructs

Mouse *Atp6v0d2* (accession no. NM_175406) and the full-length or fragments of mouse *Atp6v0a3* (accession no. NM_016921) were cloned by PCR from cDNA of mouse osteoclasts into mammalian expression vectors pcDNA3-HA and pcDNA4-Flag-Myc, respectively. For bacterial expression, coding sequences of the full-length *Atp6v0d1* (NM_013477) and *Atp6v0d2* were cloned into pGEX-4T-3 (Amersham), and the full length or fragments of *Atp6v0a3* were subcloned into pET28a (Novagen). Small hairpin RNA (shRNA) specifically targeting the mRNA of mouse *Atp6v0d2* was designed from Dharmacon siDESIGN center (http://www.dharmacon.com) with the sense strand sequences of 5′-AGAGAGUGGCAGAUAAUUA-3′ (*sh-d2-1*), 5′-UUGAAUUACUGCGCAAUAA-3′ (*sh-d2-2*), and 5′-AGACGCGCUUUAAUCAUCA-3′ (*sh-d2-3*). The sequence for shRNA targeting *LacZ* is 5′-CUCGGC GUUUCAUCUGUGG-3′ (*sh-LacZ*). The shRNA oligos were annealed and ligated into *Bgl*II/*Hin*dIII of pSUPER vector (Oligoengine), downstream of a H1 promoter. The H1-shRNA cassettes were subcloned into lentivirus vector (a kind gift from Dr. J. Kang).

Cell culture and osteoclast in vitro differentiation

Human embryonic kidney 293T (HEK-293T) and NIH-3T3 cells were maintained in DMEM supplemented with 10% FBS. Mouse BMMs and mature osteoclasts were generated as described.[21,32,33] Isolated BMMs from C57BL/6 mice were cultured in αMEM (pH 6.9) containing 10% FBS in the presence of 30 ng/ml recombinant RANKL (R&D Systems) and 30 ng/ml recombinant macrophage-colony stimulating factor (M-CSF; R&D Systems) for 5 days and characterized by staining for TRACP activity with a commercial kit (Sigma) and TRACP$^+$ MNCs were enumerated per well in a 24-well plate. Concentration of mouse cross-linked C-telopeptide of type I collagen (CTX-1) in the medium was measured with a commercial ELISA kit (cat. E0665m; Uscnlife, Wuhan, China), according to the manufacturer's procedures. The value of optical density (OD) at 450 nm of each well in the ELISA assay plate was determined using a microplate reader of SpectraMax M5 (Molecular Devices), and the concentration of CTX-1 of each well was read from a standard curve.

RNA preparation and RT-PCR

Total RNA was isolated from cultured cells or mouse tissues with TRIzol reagent (Invitrogen) according to the manufacturer's protocol. Mouse cDNA was reverse-transcribed from 0.5 mg total RNA with oligo(dT)15 primer by AMV reverse transcriptase (Promega). For real-time quantitative RT-PCR, each reaction was performed in a mixture containing EVA Green (Biotium) in a thermocycler Mastercycler ep realplex (Eppendorf), and the PCR results were analyzed with the software RealPlex (Eppendorf). Primers used for RT-PCR were as follows: *Atp6v0d1*, 5′-CCATCCGCTAGGCAGCTTT-3′ (forward) and 5′-ATCAAGGTCCTGCTCTGAGAT-3′ (reverse);

Atp6v0d2, 5′-GAAGCTGTCAACATTGCAGA-3′ (forward) and 5′-TCACCGTGATCCTTGCAGAAT-3′ (reverse); *calcitonin receptor* (*CalcR*), 5′-GACAAC TGCTGGCTGAGTG-3′ (forward) and 5′-GAAGCAGT AGATAGTCGCCA-3′ (reverse); *cathepsin K* (*CathK*), 5′-ACGGAGGCATCGACTCTGAA-3′ (forward) and 5′-GATGCCAAGCTTGCGTCGAT-3′ (reverse)[34]; *gapdh*, 5′-CTGCACCACCAACTGCTTAG-3′ (forward) and 5′-AGATCCACGACGGACACATT-3′ (reverse); β-*actin*, 5′-GAAATCGTGCGTGACATCAAAG-3′ (forward) and 5′-TGTAGTTTCATGGATGCCACAG-3′ (reverse).

GeneChip analysis

The human osteoclast cells and stromal cells were obtained as described.[19]The geneChip data were analyzed using an Affymetrix GeneChip scanner and accompanying gene expression software as described.[32]

Lentivirus production and transduction

Lentivirus vector and packaging plasmids (kindly provided by Dr. J. Kang) were co-transfected into HEK-293T cells using a calcium phosphate co-precipitation method as described.[35] Lentiviral supernatant was harvested 60 h after transfection. BMMs at RANKL induction day 1 or day 3 were transduced with lentiviral supernatant for 6 h in the presence of 4 μg/ml polybrene (Sigma). The medium was replaced with fresh αMEM containing 10% FBS, 30 ng/ml RANKL, and 30 ng/ml M-CSF for the in vitro differentiation. Transduced osteoclasts were harvested 72 h after infection and assayed for functional examinations.[32] The efficiencies of lentivirus transduction were determined by fluorescence of green fluorescent protein (GFP), which is constantly expressed from lentivirus constructs.

Cell transfection, Western blotting, and antibodies

Plasmid constructs were transfected into HEK-293T or NIH-3T3 cells using Lipofectamine reagent (Invitrogen). Cells were harvested into standard lysis buffer (50 mM Tris-HCl [pH 6.8], 100 mM dithiothreitol, 2% SDS [wt/vol], 0.1% bromphenol blue [wt/vol], 10% glycerol [vol/vol]). SDS/PAGE and Western analysis were carried out according to a standard protocol.[36] The primary antibodies used were: anti-β-actin monoclonal antibody (Sigma), anti-Flag polyclonal antibody (Sigma), anti-hemagglutinin (HA) monoclonal antibody (Sigma), anti-Myc monoclonal antibody (Santa Cruz), and anti-histidine (His) monoclonal antibody (Sigma). The rabbit antiserum specific for Atp6v0d2 was generated as described[21] against the peptide with the amino acid sequence CISQRHRTKINSYIPIL.[26] The protein levels on blot were analyzed and quantified with the NIH ImageJ software.

Cell immunofluorescence

Immunostaining of cells on coverslips or dishes directly were carried out as described[37] with antibodies as indicated (Supplementary Fig. 3). Confocal images were taken with Leica confocal TCS-SP2 from a Leica DMRE fluorescence microscope and Leica confocal software. To visualize F-actin rings, osteoclasts were stained with 2 U/ml AlexaFlour546-phalloidin (Molecular Probes). Nuclei were visualized with 1 μg/ml 4′,6-diamidino-2-phenylindole (DAPI; Sigma).

Pit formation assay and scanning electron microscopy

BMMs were grown on dentin slices (~4×4 mm^2) in the presence of RANKL/M-CSF for 5 days as described.[21,38] To visualize resorption lacunae, cells were removed from the dentin slices with 1 M ammonium hydroxide and sonication (50 Hz, 20 min). Dentin slices were washed and stained with 1% (wt/vol) toluidine blue in 1% (wt/vol) sodium borate. Pit numbers were counted under microscope, and resorption area was quantified with NIH ImageJ software. For scanning electron microscopy (SEM) analysis, dentin slices were sonicated in distilled water for 5 min and dehydrated through a graded ethanol series. Slices were coated with gold and examined with a JSM-6360 SEM (JEOL) operating at 12 kV.[33]

Acridine orange staining

Osteoclasts were incubated in αMEM containing 5 μg/ml of acridine orange (Sigma) for 15 min at 37°C, washed, and chased for 10 min in fresh media without acridine orange as described.[12,33] The cells were observed under a fluorescence microscope with a 490-nm excitation filter and a 525-nm arrest filter. The MNCs with green fluorescence from nuclei and red-orange fluorescence from acidified intra- or extracellular compartments were enumerated per well in a 24-well plate.

Microsomes preparation from osteoclasts and proton transport assay

We prepared microsomes from d2-depleted or untransduced osteoclasts as described.[29,39] Briefly, osteoclasts were washed twice with cold homogenization buffer (20 mM HEPES-KOH [pH 7.4], 1 mM EDTA, 2 mM dithiothreitol, 250 mM sucrose) at 1000*g* for 10 min at 4°C. Cells were suspended in homogenization buffer and passed 10 times through a 27.5-gauge needle. Intact cells and mitochondria were removed by centrifugation at 7000 r.p.m. for 10 min at 4°C in a Beckman SS-34 rotor. The supernatants were centrifuged at 100,000*g* for 30 min at 4°C in a Beckman SW41 rotor, and the resulting pellets were suspended in cold buffer A (150 mM KCl, 20 mM HEPES-KOH, 2 mM dithiothreitol, pH 7.4). Protein concentrations in the suspension were determined with a protein assay kit (Bio-Rad), with BSA as a standard.

We performed the proton transport assay as described.[21,29,39] We incubated microsome samples from osteoclasts (~15 μg) for 7 min in 2 ml acidification buffer (150 mM KCl, 20 mM HEPES-KOH, 5 mM $MgCl_2$, 5 μM acridine orange, 1.25 μM valinomycin, pH 7.4) at 25°C. Proton transport was initiated by addition of ATP and monitored as fluorescence quench of acridine orange (excitation, 492 nm; emission, 520 nm) using a fluorescence spectrophotometer of Varian, and data were analyzed with Cary Eclipse Kinetics software (Varian). The initial rate

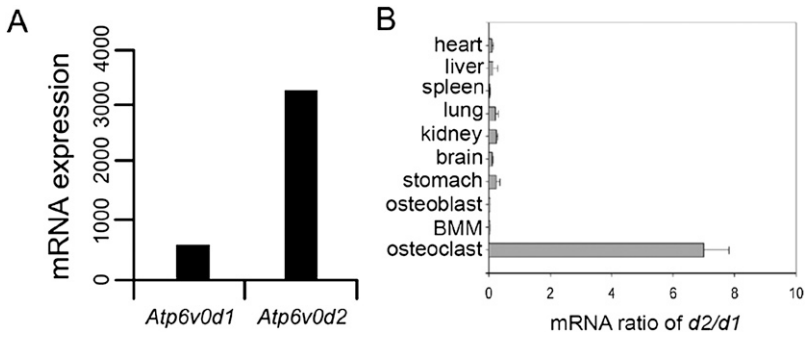

FIG. 1. Expression of *Atp6v0d2* in mature osteoclasts. (A) Comparison of microarray data for expression levels of *Atp6v0d1* and *Atp6v0d2* in human osteoclasts. (B) Ratios of the mRNA levels of *d1* and *d2* in mouse tissues and related cells assessed by real-time RT-PCR. The value of *d2*/*d1* is the ratio of transcript copy numbers from the two genes measured in an equal amount of cDNA template ($n = 3$).

(ΔF/min) was derived from the slope generated by the first 60 s of the acidification assay. We also determined the total fluorescence change after addition of 1.5 μM nigericin (ΔF). Valinomycin and nigericin were purchased from Sigma.

Co-immunoprecipitation assay

HEK-293T cells transfected with the mammalian expression constructs pcDNA-HA-d2 and pFlag-a3F-Myc were lysed in IP lysis buffer (20 mM Tris-HCl [pH 7.4], 150 mM NaCl, 1% Nonidet P40 [vol/vol], 1 μg/ml leupeptin, and 1 mM phenylmethanesulfonyl fluoride [PMSF]), sonicated briefly (100 W; 10 s on/15 s off; 10 cycles), and cleared by centrifugation at 10,000*g* for 10 min at 4°C as described.[40] Supernatants were incubated with anti-Myc or anti-HA monoclonal antibodies at 4°C for 2 h. Protein G-agarose beads (Roche) were added into the mixture and rotated at 4°C overnight. Immunoblotting was performed as described above with anti-d2 rabbit antiserum and anti-Flag polyclonal antibody, respectively.

Protein expression, purification, and GST pull-down assay

GST and histidine-tagged fusion proteins were expressed in the *E. coli* strain BL21 (DE3). Purification was performed using glutathione-Sepharose 4B (Amersham) for GST fusion proteins or Ni^{2+}-nitrilotroacetate (Ni-NTA) column (Qiagen) for His-tagged proteins as described in the manufacturer's instructions, following the induction of the cells with 0.2 mM isopropyl *b*-D-thiogalactopyranoside (IPTG) at 16°C for 20 h.

The GST pull-down assay was performed essentially as described.[36] Ten micrograms GST or GST fusion proteins purified from bacteria was incubated with glutathione-Sepharose 4B beads (Amersham) in the binding buffer (0.2% Nonidet P40 [vol/vol], 1% BSA [wt/vol], 1 mM dithiothreitol, 1 mM PMSF, in 1× PBS) in a total volume of 500 μl at 4°C for 2 h. Fifteen micrograms of purified His fusion proteins was added to the slurry and incubated at 4°C for another 2 h. The Sepharose beads were washed with the wash buffer (20 mM Tris-HCl [pH 8.0], 300 mM NaCl, 0.5% Nonidet P40 [vol/vol], 1 mM EDTA, 1 mM PMSF) three times, and bound proteins were resolved by SDS/PAGE and visualized by Western blotting using anti-histidine antibody.

Statistical analysis

All data are expressed as mean ± SD from at least three independent experiments for each experimental condition. Statistical analysis was evaluated with paired Student's *t*-test to analyze differences between groups. The graphs and plots were produced with Sigmaplot software (Systat Software).

RESULTS

High expression of Atp6v0d2 in matured osteoclasts

We characterized Atp6v0a3 (a3, Atp6i, Tcirg1) as an osteoclast-specific isoform of subunit a in V-ATPase that is essential in osteoclast-mediated extracellular acidification.[20,21] In this study, we tried to characterize other osteoclast proton pump subunits using microarrays to analyze gene expression profiles in mature osteoclasts as described.[30–32] We found that the expression level of Atp6v0d2 (d2), one isoform of subunit d in V-ATPase, was induced ~100-fold with RANKL, whereas expression of Atp6v0d1 (d1), another isoform of subunit d, could not be induced (data not shown). In addition, the level of d2 expression was ~5-fold higher than that of d1 in human mature osteoclasts, indicating that d2 may function as an osteoclast-specific subunit in V-ATPase like a3 (Fig. 1A).

The subunit d2 has been identified in various tissues, with the most abundance in osteoclasts.[15,16] Similar to a3, we observed the upregulation of d2 expression in osteoclast differentiation from BMMs in vitro (Supplementary Fig. 1A, left), as previously reported.[29] Similar to the microarray data from human osteoclasts, the transcription level of d2 was ~7-fold higher than d1 in mouse mature osteoclasts shown in the mRNA ratio of d2/d1 quantified with real-time RT-PCR experiments, whereas the ratios in other mouse tissues were much lower in the comparison (Fig. 1B). Notably, $TRACP^+$ typical MNCs formed at day 4 have been shown to have similar mRNA levels of d2 and two osteoclast marker genes (i.e., *CalcR* and *CathK*) as those at the later stage of day 5 (Supplementary Figs. 1B and 1C). However, protein levels of Atp6v0d2 expression increased dramatically from day 4 to day 5 (Supplementary Fig. 1A, right). Taken together, the results suggested that d2 may be functionally important in matured osteoclasts.

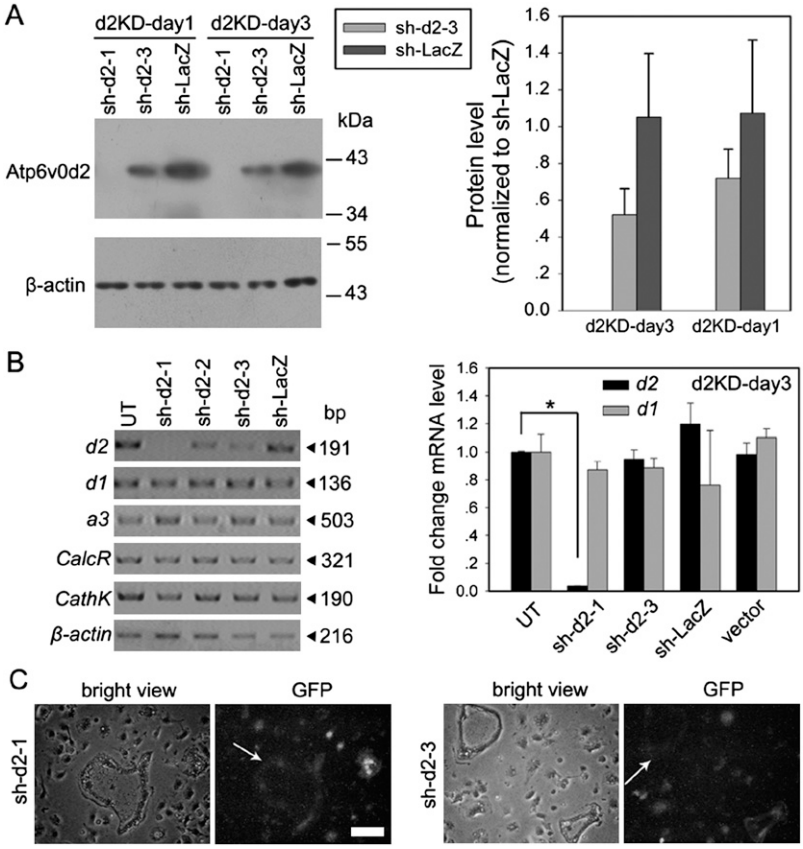

FIG. 2. Lentivirus-mediated differentiation stage-specific RNAi of *Atp6v0d2*. (A) Depletion of Atp6v0d2 with lentiviral shRNA shown in protein expression level. (Left) Western blotting shows the depletion of d2 in d2KD-day1 and -day3 osteoclasts transduced with lentivirus encoding shRNA of *Atp6v0d2* (*sh-d2-1* and *sh-d2-3*) and *LacZ* (*sh-LacZ*) or lentiviral empty vector (vector). (Right) Quantitative analysis of protein levels in left. Protein levels on blot were analyzed with NIH Image software, and the data were normalized to *sh-LacZ*, respectively ($n = 3$). (B) Lentiviral depletion of d2 in d2KD-day3 osteoclasts shown in mRNA level. (Left) RT-PCR showed the expression of related genes in d2KD-day3 osteoclasts. Arrowheads indicate the sizes of PCR products. (Right) quantification of the mRNA levels of *d1* and *d2* (normalized to the β-*actin* level) in d2KD-day3 osteoclasts by real-time RT-PCR. Shown are the averages and SDs of relative values compared to untransduced (UT) osteoclasts ($n = 3$). *$p < 0.01$. (C) The high transduction efficiency of lentivirus encoding different shRNA in d2KD-day3 osteoclasts indicated by the GFP fluorescence compared with the bright views. Arrows indicate GFP^+ MNCs. Scale bar = 30 μm.

Atp6v0d2 knockdown by lentivirus-mediated differentiation stage-specific RNAi during osteoclast differentiation

The poor formation of MNCs with abnormal resorptive capability derived from *Atp6v0d2*$^{-/-}$ BMMs precludes the possibility to study d2 function in mature osteoclasts.[29] Here we adopted a lentivirus-based knockdown approach at different stages in RANKL-induced osteoclast differentiation to define whether d2 is required for the function of matured osteoclasts beyond its critical involvement in the cell maturation process.[32] To address this point, d2 expression was depleted by lentiviral shRNA transduction at early or late stages. RANKL induction day 3 was chosen as the late stage for d2 knockdown (designated as d2KD-day3) as indicated by the emergence of MNCs in observation (Supplementary Fig. 1B) and by the expression patterns of specific osteoclast marker genes (Supplementary Fig. 1C). As a control experiment to confirm the role of d2 in osteoclast maturation, knockdown of d2 was also carried out at day 1 (designated as d2KD-day1), which was chosen as the early stage in differentiation as indicated by the expression patterns of marker genes (Supplementary Fig. 1C). After lentivirus transduction, osteoclasts in both knockdown treatments were induced with RANKL until day 5 for further analyses.

One of three shRNA targeting coding sequences of *Atp6v0d2* (*sh-d2-1*) was validated for the effective plasmid-based knockdown of overexpressed d2 cDNA in HEK-293T cells (Supplementary Fig. 1D). This shRNA was subcloned into a lentiviral vector for the virus-based knockdown experiment, as were three other shRNA (*sh-d2-2, sh-d2-3,* and *sh-LacZ* targeting *LacZ* gene). These were carried out as off-target controls for d2 depletion. A previous report has shown the efficiency of lentivirus transfection to be <50%.[41] However, as shown in Fig. 2C, we found that the transduction efficiencies were almost 100% (indicated by the green fluorescence of GFP that was constantly expressed in the lentivirus vector) for all experimental groups of d2KD-day3 (Fig. 2C) and of d2KD-day1 (Supplementary Fig. 2J). We speculate that this discrepancy might come from different lentivirus titers, multiplicity of infection (MOI), and targeting cells because human osteoclasts were used in the previous report.[41] Convincingly, another report has also recently shown a transduction of nearly 100% of the lentivirus into mouse primary osteoclasts.[23]

Western blotting showed that protein levels of d2 were repressed by lentiviral *sh-d2-1* transduction in both d2KD-day3 and d2KD-day1 osteoclasts (Fig 2A, left). The transcription level of d2 in lentiviral *sh-d2-1* transduction was greatly decreased, whereas d1 remained stable (Fig. 2B, left; Supplementary Fig. 1E, left). Real-time RT-PCR further showed that mRNA levels of d2 in d2KD-day3 or -day1 (*sh-d2-1*) were reduced to ~4% of those in untransduced osteoclasts (UT; Fig. 2B, right; Supplementary

Fig. 1E, right). In contrast, lentiviral transduction of *sh-d2-3* and *sh-LacZ* only showed compromised depletion effects on d2 expression with ~20% for *sh-d2-2* (80% of d2 expression remained) and even lower for *sh-d2-3* (~50% in protein level as shown in Fig. 2A, right). The control *sh-LacZ* did not have any depletion effects on d2 expression in protein or mRNA level and neither did the lentiviral empty vector (vector; Figs 2A and 2B). This suggests none or few interference effects from those lentiviruses. In addition, lentivirus infection seemed to not hamper expression of other proton pump subunits in osteoclasts, including d1 and a3, or other osteoclast marker genes, such as *CalcR* and *CathK* (Fig. 2B and Supplementary Fig. 1E, left). Collectively, these results showed the high transduction efficiency of lentivirus into primary osteoclasts and the effective depletion of d2 with lentiviral shRNA at both the early and late stages in osteoclast differentiation.

Normal maturation of d2KD-day3 osteoclasts

We examined whether the depletion of d2 affected maturation in d2KD-day3 or -day1 osteoclasts in a like manner to osteoclast differentiation in *Atp6v0d2*$^{-/-}$ mice.[29] First, when d2KD-day3 osteoclasts knocked down by *sh-d2-1, sh-d2-3*, or *sh-LacZ* were induced with RANKL to day 6, the cell morphology and viability seemed to be similar to control cells (data not shown). Because both the vector and UT controls have normal osteoclast morphology, the lentiviral manipulation did not hamper the normal differentiation of osteoclasts (Fig 2B, left). Next, we examined the expression of an osteoclast marker gene *TRACP* in d2KD-day3 cells with a TRACP staining method.[33] The similar patterns of red-stained MNCs (TRACP$^+$ mature osteoclasts) were shown among *sh-d2-1* (Fig. 3A), *sh-d2-3*, *sh-LacZ* (Figs. 3B and 3C), and UT (Fig. 3F), with the average numbers of TRACP$^+$ MNCs (at least three nuclei) enumerated in these osteoclasts around 120.0–136.3 per well of a 24-well plate (Fig. 3K). Notably, numbers of all TRACP$^+$ cells including mononuclear pre-osteoclasts were also quantified comparable in these groups, suggesting that the ratios of MNCs fusion were similar in d2-depleted cells and normal expressed cells (Fig. 3L). TRACP staining was also assayed on osteoclasts grown on dentins, bone slices, to mimic a more physiological condition for the activity of the acid phosphatase.[31] Convincingly, we saw similar TRACP staining patterns (data not shown) and TRACP$^+$ MNCs proportions between *sh-d2-1* and other groups (Fig. 3M). The results above showed that the deficiency of d2 in a late stage of osteoclast differentiation does not affect the maturation of osteoclasts. In contrast, a decreased number of TRACP$^+$ MNCs (Fig. 3D) and reduced proportion of MNCs in population (Figs. 3K and 3M) were found in *sh-d2-1* osteoclasts of d2KD-day1 (15.7 ± 5.0), indicating the efficiency of d2 depletion compared with the normal maturation of *sh-d2-3* cells (Fig. 3E). This result suggests that d2 is essential in an early differentiation stage as shown in the mouse model.[29]

On activation, after attachment to the matrix surface (i.e., dentin slice or plastic dish), a mature osteoclast could be ''resorption capable'' within its ruffled border. The resorption site is rich in filamentous actin (F-actin) where quantities of V-ATPases reside and transport protons actively.[1,32] Because the deficiency of C1 could disrupt the formation of F-actin rings, we examined the integrity of the actin ring to define whether d2-depleted osteoclasts were indeed actively ready with a ruffled border.[23,42] Staining of d2KD-day3 osteoclasts with AlexaFlour546-phalloidin (Molecular Probes) showed normal F-actin rings with red fluorescence emission either in *sh-d2-1* or in vector (Figs. 3G and 3H), with the average ring numbers in all experimental groups around 153.3–177.7 per well (Fig. 3N). As expected, the formation of actin rings was indeed decreased in d2KD-day1 osteoclasts (Figs. 3I and 3J). The average number in *sh-d2-1* was reduced to 20.9 ± 5.2 (compared with UT: 174.2 ± 25.8; Fig. 3N), which indicated less formation of mature osteoclasts, as was observed in *Atp6v0d2*$^{-/-}$ osteoclasts.[29] The staining of F-actin rings of MNCs on dentin slices had similar results (data not shown). In summary, the results showed that d2KD-day3 osteoclasts showed normal differentiation and maturation from the loss-of-function study of Atp6v0d2.

Deficiency of d2 impairs the bone resorption of osteoclasts

The results above collectively hint at a different role of d2 beyond cell fusion in osteoclasts that have already matured. As such, we anticipated that d2 may also play a role in bone resorption, the major function of osteoclasts.[1] To address this point, we performed a pit formation assay to directly assess the resorption ability of d2-depleted osteoclasts by comparing the resorption lacunae termed ''pits'' on dentin surfaces produced by osteoclasts grown on the bone slices.[33] As shown in d2KD-day3 osteoclasts, staining with toluidine blue (Sigma) showed the poor formation of blue-stained resorption pits in *sh-d2-1* (Fig. 4A). In contrast, *sh-d2-3, sh-LacZ*, and UT showed numbers of blue-stained, irregular-shaped resorption pits with various sizes of surface spread across the dentins (Figure 4B–D). The same result was found in d2KD-day1 osteoclasts with a sharply decreased pit formation in *sh-d2-1* (Supplementary Figs. 2E and 2G).

We quantified the large lacunae ($\geq$4000 μm^2) in d2KD-day3 osteoclasts to rule out the contributions of mono- and di-nucleated pre-osteoclasts, which may also participate in the formation of resorption lacunae of small sizes.[2] Osteoclasts from *sh-d2-3*, *sh-LacZ*, or UT produced ~13.0–19.0 large pits per dentin (4×4 mm^2), whereas the average pit number of *sh-d2-1* was reduced to 2.0 ± 1.0 and only 11.3% of that in vector (17.7 ± 2.5; Fig. 4J). Similarly, the number was reduced lower to 1.3 ± 1.5 for *sh-d2-1* in d2KD-day1 osteoclasts and only 7.5% of that of vector (Fig. 4J). Despite some contributions to bone resorption of the MNCs already emerged at day 3, it is obvious that the impairment of bone resorption was not caused by the decrease in MNCs formation but ascribed to the d2 depletion. Besides, when we enlarged the counting to include those small lacunae (<4000 μm^2), compromised resorption ability was also found in d2KD-day3 or -day1 osteoclasts,

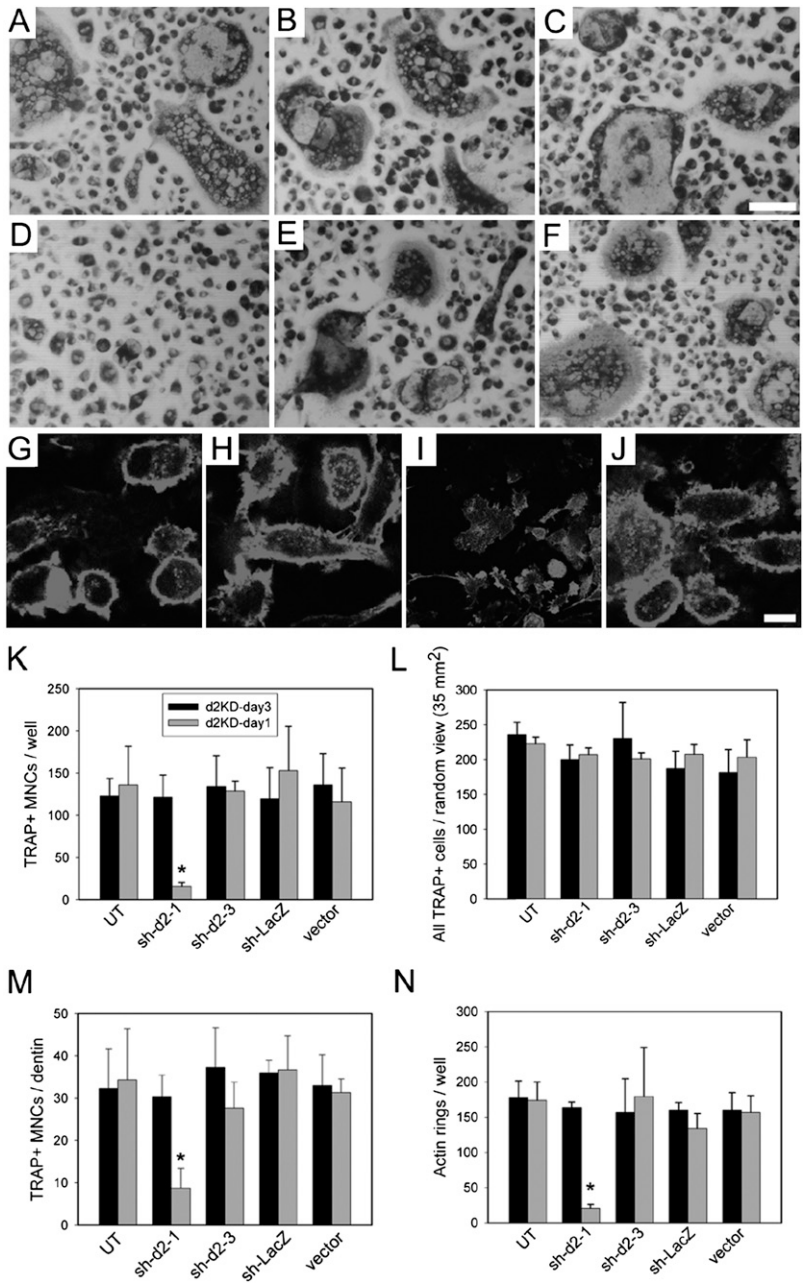

FIG. 3. Normal maturation of d2KD-day3 osteoclasts. (A–C) TRACP staining of d2KD-day3 osteoclasts. (A) *sh-d2-1*. (B) *sh-d2-3*. (C) *sh-LacZ*. (D and E) TRACP staining of d2KD-day1 osteoclasts. (D) *sh-d2-1*. (E) *sh-d2-3*. (F) TRACP staining of untransduced osteoclasts. (G–J) Immunostaining of F-actin rings with Alexa-Fluor546-phalloidin in d2KD-day3 osteoclasts for (G) *sh-d2-1* and (H) vector and in d2KD-day1 osteoclasts for (I) *sh-d2-1* and (J) vector. (K) Quantification of $TRACP^+$ MNCs (at least three nuclei) per well. (L) Quantification of all $TRACP^+$ cells per random view (35 mm^2). (M) Quantification of $TRACP^+$ MNCs per dentin slice. (N) Quantification of F-actin rings per well. All data are expressed as mean ± SD ($n = 3$). $^*p < 0.05$. Scale bars = 30 μm.

indicating that the depletion of d2 also impaired the bone resorption in pre-osteoclasts (Fig. 4K). Because the area of each pit greatly varies and it is usually hard to distinguish an individual pit from neighboring pits, we also compared the total resorbed area with the whole dentin surface (4×4 mm^2; analyzed with NIH ImageJ software). The coverage of resorption lacunae on dentin was decreased to around only 4.3% for *sh-d2-1* in d2KD-day3 or 1.7% in d2KD-day1 osteoclasts, respectively. In contrast, the relevant percentages for control groups were ~33.3–43.0% (Fig. 4L).

We also confirmed the resorption data with a JSM-6360 SEM (JEOL). As shown in Fig. 4, reduction of lacunae formation in *sh-d2-1* was observed in ×500 images (Figs. 4E and 4G), and the surface area and depth of typical resorption pits were also shown in more enlarged pictures (Fig. 4H, ×1000; Fig. 4I, ×5000). Similar results were also shown in d2KD-day1 osteoclasts (Supplementary Figs. 2H and 2I). We also examined the concentration of mouse CTX-1 in the culture medium, which was determined with an ELISA kit as a direct measure of resorptive activity of osteoclasts. The concentration of CTX-1 in *sh-d2-1* was also much reduced in d2KD-day3 or -day1 compared with other control groups (Fig. 4K). In all these quantitative data related to bone resorption, the *sh-d2-3* did not show obvious impairments (if any, it was only a very slight decrease) of the resorption ability of osteoclasts. This

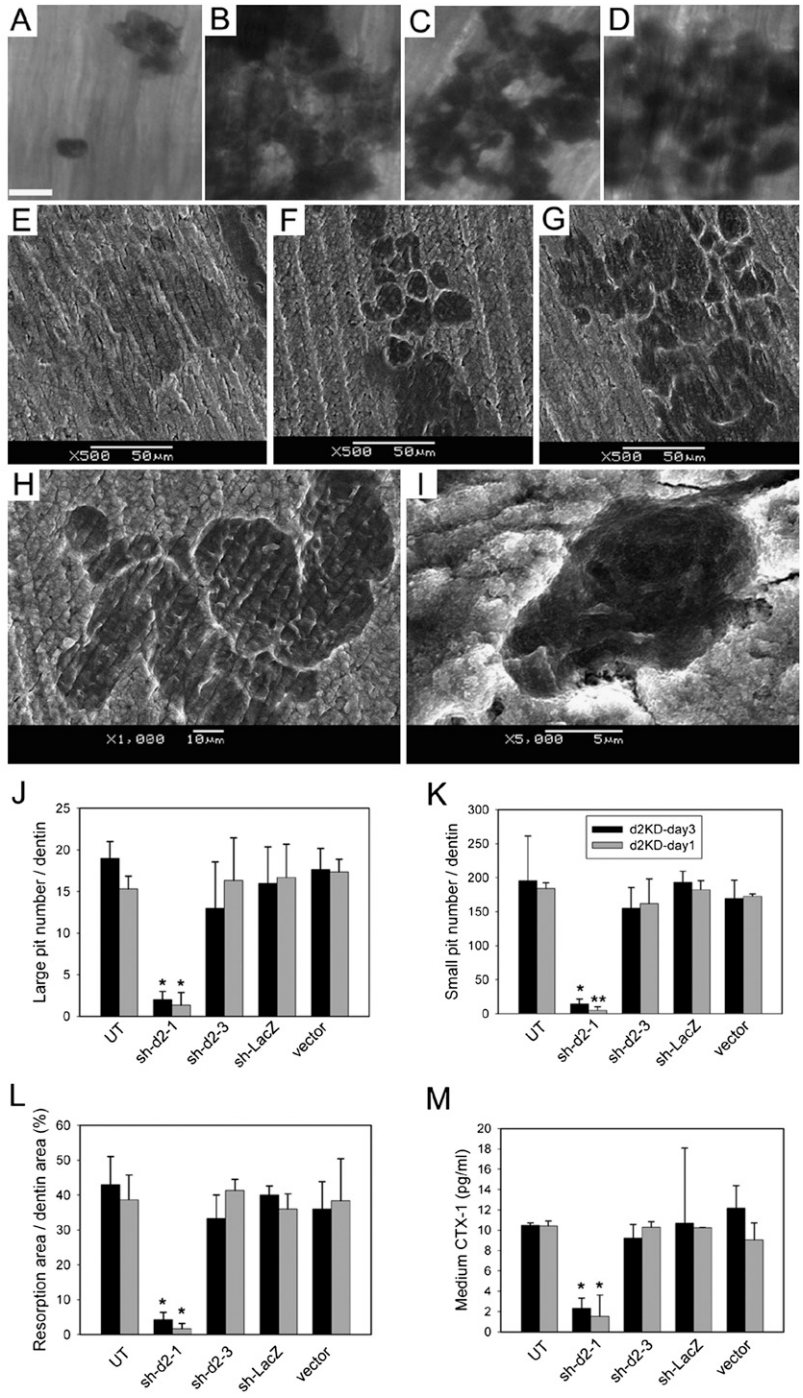

FIG. 4. Impaired activity of bone resorption in d2KD-day3 osteoclasts. (A–D) Formation of resorption pits in d2KD-day3 osteoclasts on dentin slices for (A) *sh-d2-1*, (B) *sh-d2-3*, (C) *sh-LacZ*, and (D) UT, respectively. Scale bar = 30 μm. (E–I) Resorption lacunae were visualized by SEM. ×500 pictures shown for (E) *sh-d2-1*, (F) *sh-d2-3,* and (G) UT. (H) Large resorption lacuna (*sh-LacZ)* was shown in detail in ×1000 picture. (I) Small resorption lacuna (vector) was shown in detail in ×5000 picture. (J) Numbers of the large resorption pits (≥400 μm^2) per dentin slice. (K) Numbers of the small resorption pits (<400 μm^2) per dentin slice. (L) The resorption areas of pits were determined using NIH *ImageJ* software. (M) Medium type 1 collagen cross-linked telopeptide (CTX-1) measured by ELISA. All data are expressed as mean ± SD ($n = 3$). *$p < 0.05$; **$p < 0.01$.

suggests that the partial depletion of d2 may not hamper its functions as in cell fusion (Fig. 3). In summary, our results show that d2 is needed for the bone resorption of osteoclasts.

Depletion of d2 affects the extracellular acidification of osteoclasts

Bone resorption by osteoclasts is attributed to an extracellular acidified compartment inside ruffled borders that is supported by the proton-pumping V-ATPase complexes in plasma membrane.[9,12] To define if d2, an isoform of subunit d of V-ATPase, contributes to the extracellular acidification of osteoclasts such as a3,[21] we applied an acridine orange staining assay on d2KD-day3 cells, which could show the intra- or extracellular acid compartments present with the indicative orange or red fluorescence.[21] As shown in d2KD-day3 MNCs, red fluorescence from vector or other control groups appeared both in cytoplasm and around the plasma membrane

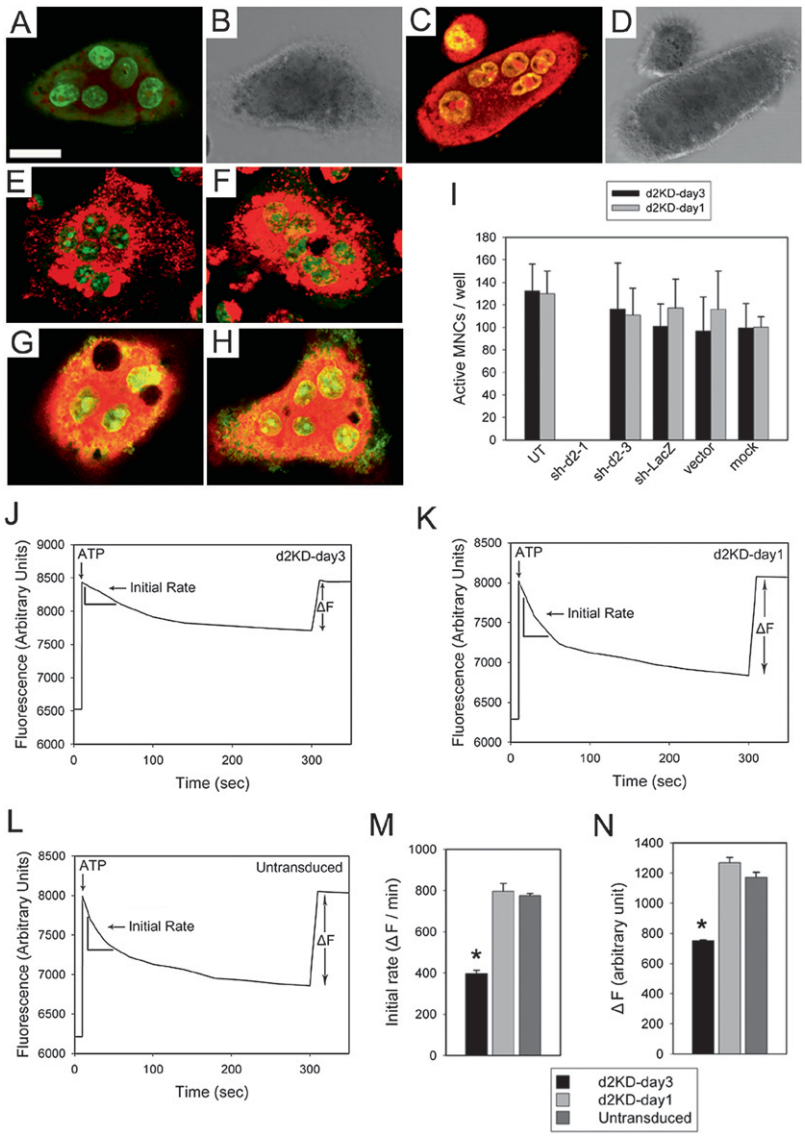

FIG. 5. Impaired extracellular acidification in d2KD-day3 osteoclasts. (A–H) Vital staining of d2KD-day3 MNCs with acridine orange for (A) *sh-d2-1*, (C) vector, (E) *sh-d2-3*, (F) *sh-LacZ*, (G) mock, and (H) UT, respectively. The bright views (B) for A and (D) for C are also shown. Scale bar = 10 μm. (I) Quantification of MNCs with active extracellular acidification per well. (J–L) Proton transport assays on microsomal preparation of (J) d2KD-day3 and (K) d2KD-day1 osteoclasts transduced with *sh-d2-1* lentivirus. Microsomes from untransduced osteoclasts were assayed as control (L). (M) Comparison of initial rates of the proton flux in the first 60 s after adding 1.5 mM ATP in J–L. (N) Comparison of total acidification (shown as ΔF) in J–L. All data are expressed as mean ± SD ($n = 3$). *$p < 0.05$.

(Figs. 5C–5H), indicating the active acid production of V-ATPase both in the intracellular organelles and across the plasma membrane. In contrast, only spotted red fluorescence was observed in cytoplasm of *sh-d2-1,* with a lack of acidification in extracellular compartments around the plasma membrane (Figs. 5A and 5B). The proton-pumping across the plasma membrane was almost abolished because the number of MNCs with active extracellular acidification in *sh-d2-1* was reduced to <1% of that in control vector (Fig. 5I). Similar to *Atp6v0a3*$^{-/-}$ osteoclasts, the results indicate severe impairment of V-ATPase activities in the plasma membrane of osteoclasts because of the deficiency of d2 expression.[21] Nevertheless, these cells seemed able to be normally activated with the formation of F-actin rings (Figs. 3G–3J). The acridine orange staining assay on d2KD-day1 cells showed a decrease in MNC formation (Supplementary Figs. 2A–2D) caused by the deficiency of d2 expression at an early differentiation stage. Interestingly, orange fluorescence was also absent in extracellular compartments around the plasma membranes of those mono- or di-nucleated pre-osteoclasts in *sh-d2-1* (Supplementary Figs. 2A and 2B), implying that the impairment of extracellular acidification might also affect those premature osteoclasts. Again, we did not find any effects from *sh-d2-3* or *sh-LacZ* on the extracellular acidification (Figs. 5E and 5F), suggesting the specificity of *sh-d2-1* in the loss-of-function of d2.

To confirm the impairment of acidification in d2-depleted osteoclasts more quantitatively, we also applied the proton transport assay as described.[21,29,39] Microsomes from d2KD-day3 or -day1 osteoclasts, as well as untransduced osteoclasts, were prepared. There was considerably less microsomes of d2KD-day1 (about one half of those in d2KD-day3 or UT), possibly because of a reduced formation of MNCs. In proton transport assays, we put 15 μg of the microsomes into reaction buffer, and the ATP-driven

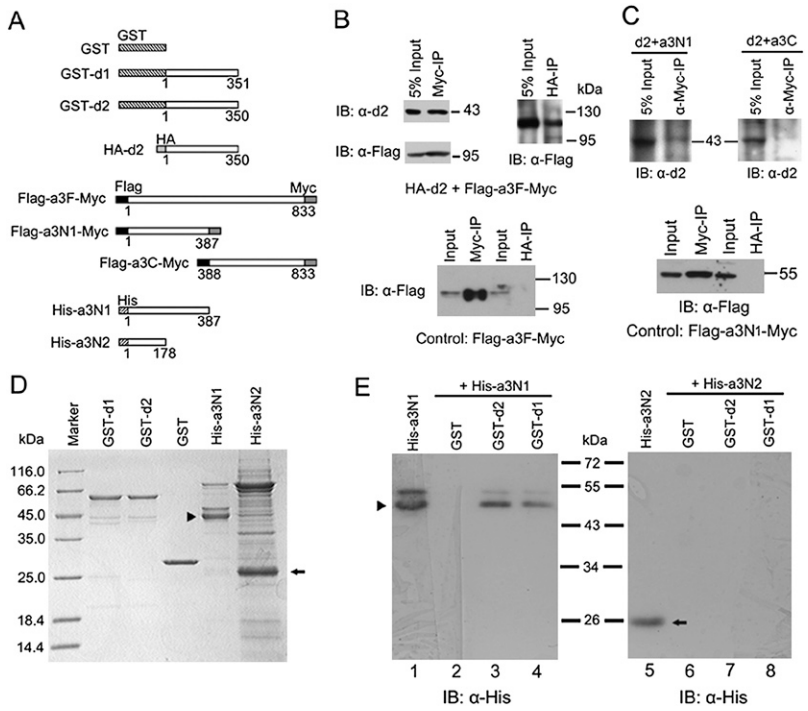

FIG. 6. Association of Atp6v0d2 and proton pump subunit Atp6v0a3. (A) Full-length or fragments of d1, d2, and a3 tag-fusion proteins. GST, HA, Flag, Myc, and His tags are shown above each bars. The numbers indicated below each bars show the amino acid coordinates of the polypeptide regions relative to the corresponding full-length proteins. (B) Co-immunoprecipitation (Co-IP) of Atp6v0d2 with Atp6v0a3 expressed from transfected cells. HEK-293T cells were transiently transfected with pcDNA3-HA-d2 and pFlag-a3F-Myc alone (bottom) or in combination (top). Whole cell extracts were immunoprecipitated (IP) with anti-Myc or anti-HA antibody. The precipitated proteins were analyzed by immunoblotting (IB) using anti-d2 or anti-Flag antibody as indicated. (C) HA-d2 associates with Flag-a3N1-Myc but not Flag-a3C-Myc in Co-IP assay (top). Single transfection of pFlag-a3N1-Myc was also carried out as IP control (bottom). (D) Proteins used for GST pull-down assay. Five percent input for all tagged proteins were purified from *E. coli* strain BL21 (DE3), resolved in SDS-PAGE, and visualized with Coomassie Blue staining. (E) Direct interaction of d2 with a3N1 but not with a3N2. Western blotting analysis using anti-His antibody of the His-tagged a3N1 and a3N2 in fractions obtained from GST pull-down assays using GST (lanes 2 and 6), GST-d2 (lanes 3 and 7), or GST-d1 (lanes 4 and 8). Five percent of the input His-tagged proteins were loaded (lanes 1 and 5). Arrowheads indicate His-a3N1 and arrows indicate His-a3N2 in D and E.

initial rates of proton flux (ΔF/min) along with the total acidification (ΔF) were generated from plots (Figs. 5J–5L). We found both values of d2KD-day3 to be lower than d2KD-day1 or UT with a significant difference ($p < 0.05$). These results suggest that the impairment of proton transportation of d2KD-day3 was caused by the failure of V-ATPase and not by a low formation of MNCs (Figs. 5M and 5N). Because V-ATPases in normal multinucleated osteoclasts would be present in greater abundance in the plasma membrane than in intracellular compartments,[39] the reduced V-ATPase activity probably resulted from the decreased extracellular acidification caused by d2 depletion. Strikingly, the activity of proton transport was similar in d2KD-day1 and UT. This is in accordance with the previous report from a gene targeting study of d2.[29] We speculated that with the same amounts of microsomes in this experiment, the comparable pumping activity of d2KD-day1 with UT was probably caused by the contribution of the intact d1-integrated V-ATPase in intracellular compartments (Figs. 5A and 5B). In summary, our results suggest that d2 may be involved in the extracellular acidification of V-ATPase across the plasma membrane of osteoclasts.

Association of Atp6v0d2 and Atp6v0a3

Our results above indicate that d2 may be required for the extracellular acidification of V-ATPase. However, determining whether d2 is a true component of the proton pump and identifying the molecular mechanism by which d2 regulates the extracellular proton-pumping process in the complex still need to be further addressed. Previous studies have shown the localization of d2 in the ruffled border where it co-localizes with subunit a3 in human osteoclasts.[26] The interaction between subunit d and B in kidney cells has also been reported in Co-IP experiments,[43] indicating that d2 may integrate into V-ATPase of osteoclasts by direct interaction with other osteoclast-specific subunits. Therefore, we performed a Co-IP assay to examine the interaction between the mouse proteins d2 and a3, which is the only functionally characterized osteoclast-specific subunit thus far.[21,22] Indeed, we found the fusion protein HA-d2 could be precipitated by Flag-a3F-Myc (the fusion protein of full-length a3) in HEK-293T cells and vice versa (Fig. 6B). The 116-kDa protein a3 (aa 1–833) contains an N-terminal cytosolic region facing the cytoplasm and a C-terminal nine trans-membrane domain

integrated across the plasma membrane.[44,45] Therefore, we next examined the interaction between d2 and a3N1 (aa 1–387 of a3), the N-terminal to the first putative transmembrane helix, and between d2 and a3C (aa 388–833), the C-terminal domain containing the nine transmembrane helixes, using Co-IP assays (Fig. 6A).[45] HA-d2 could associate with Flag-a3N1-Myc, although the interaction seemed to be much weaker than with a3F (Fig. 6C). In contrast, we could not detect the co-precipitation of HA-d2 and Flag-a3C-Myc (Fig. 6C). As such, the data suggest that a3 may bind d2 at the amino terminal cytosolic domain.

We also carried out the Co-IP assay in primary osteoclasts to examine the endogenous interaction between d2 and a3. However, because of the lack of good antibodies of d2 and a3 for Co-IP, we could not further define the association profile of the two subunit isoforms in endogenous proton pumps. Instead, we used a GST pull-down assay to examine the direct interaction between d2 and its fragments (Fig. 6A). The His-tagged full-length a3F and a3C could not be expressed in *E. coli*, probably because of the insolubility of the proteins (data not shown). Nonetheless, GST fusion proteins GST-d1 or GST-d2 and His-tagged proteins His-a3N1 or His-a3N2 (aa 1–178) could be expressed and purified from the *E. coli* strain BL21(DE3) (Fig. 6D). We found that both d1 and d2 did associate with a3N1 directly, although the interaction with a3N1 seemed more extensive for d2 than d1 (Fig. 5E, left). This suggests a more specific binding of d2 and a3 in osteoclasts. In contrast, neither d1 nor d2 could interact with a3N2, following the GST pull-down even with much longer exposure for the blots, as shown with Western blotting analysis (Fig. 5E, right). As far as we know, these results are the first report thus far about the direct interaction between d2 and other osteoclast-specific pump subunits.

We also visualized the subcellular localization profiles of HA-d2 and Flag-a3F-Myc in NIH-3T3 cells using immunostaining with corresponding antibodies for the fusion tags. Because a3 has been proven to localize to late endosomes and lysosomes in NIH-3T3 cells,[46] if d2 interacts with a3, it should also localize to these intracellular organelles. Flag-a3F-Myc seemed to reside mainly, if not exclusively, punctually in the cytoplasm (Supplementary Fig. 3, first panel), similar to the distribution of HA-d2 in NIH3T3 cells (Supplementary Fig. 3, second panel). When simultaneously expressed in NIH-3T3 cells, HA-d2 and Flag-a3F-Myc seemed to co-localize in cytoplasm with punctual pattern (Supplementary Fig. 3, third panel), suggesting the probable association between d2 and a3 in the lysosomes. In summary, our results above provide evidence of the possible interaction between the two osteoclast-specific subunits d2 and a3.

DISCUSSION

Atp6v0d2 was characterized in our search for osteoclast-specific subunits of V-ATPase serving in bone resorption of osteoclasts.[31,32] Despite its distribution in various tissues including kidney and liver,[15,16,26] d2 has a prominent expression profile in osteoclasts (Fig. 1). Targeted disruption of d2 in mice led to an osteopetrosis phenotype that was similar to the *Atp6v0a3*$^{-/-}$ mice,[21] suggesting its essential role(s) in osteoclasts. However, although a3 has been characterized as a functional component of V-ATPase, d2 involvement was attributed to pre-osteoclast fusion.[29,47] To define the role of d2 in V-ATPase activity, we performed a differentiation-stage specific depletion of d2 in mouse osteoclast induction in vitro (Fig. 2) instead of the global inactivation of d2 in mice. In accordance with the increasing expression profile in osteoclast differentiation (Supplementary Fig. 1), d2 has been shown to have dual functions in pre-osteoclast fusion at an early differentiation stage (Figs. 3D and 3E) and in extracellular acidification at the late stage of mature osteoclasts (Fig. 5). Besides, we applied two more shRNA to d2 (*sh-d2-2* and *sh-d2-3*) and the shRNA to *LacZ* gene (*sh-LacZ*) as off-target controls of the effective shRNA of d2 (*sh-d2-1*). Approximately, the *sh-d2-2* shRNA had a 20% silencing effect on the depletion of d2 expression (data not shown), and the *sh-d2-3* shRNA had a 50% silencing effect on the depletion of d2 protein expression (Fig. 2A, right). However, the shRNA to *LacZ* gene (*sh-LacZ*) did not have an effect on the depletion of d2 expression (Fig. 2) nor did it impair the maturation (Fig. 3) and normal function of osteoclasts in our experiments (Figs. 4 and 5). These data excluded the possibility of shRNA off-target effects of *sh-d2-1* (i.e., its effects were indeed d2 knockdown specific). In addition, the association of d2 and a3 in both the GST pull-down and Co-IP assays (Fig. 6) adds proof to the hypothesis that osteoclasts select a particular combination of subunit isoforms to form the V-ATPases in plasma membrane that are specifically needed for extracellular acidification.[7]

Diversity of subunit d in osteoclasts

It has been clear that a given cell type can have multiple subunit isoforms, such as d1 and d2 characterized in osteoclasts.[15] Despite ~67% identical amino acid sequences, they seem to function diversely: a more ubiquitous role of d1 based on its comparable expression levels in most mouse tissues analyzed using RT-PCR (data not shown) and a more specialized role(s) of d2 suggested by the dominant expression of d2 in osteoclasts (Fig. 1). Furthermore, by carefully comparing expression levels of d1 and d2 using real-time RT-PCR, we repeatedly found that d2 was highly induced by RANKL during osteoclast differentiation (Supplementary Fig. 1A). In mature osteoclasts, the expression level of d2 is 5-fold (in humans) or 7-fold (in mice) higher than d1 (Fig. 1). However, in a recent report by Lee et al.,[29] the d1 level was much higher than d2. Currently, we do not know the cause of this difference. The expression patterns of high induction and high expression indicate the potentially important role of d2 in osteoclast bone resorption as one subunit of the proton pump. Our study shows that d2 function is essential for the extracellular acidification of osteoclasts.

We speculate that d1 is also expressed in the osteoclast and that it may ubiquitously contribute to the common V-ATPase activity in intracellular organelles in osteoclasts as it does in other cell types,[15] whereas d2 may serve mainly in proton-pumping across the plasma membrane only in activated osteoclasts (Fig. 3J). In support of this

hypothesis, gene disruption of *Atp6v0*d1 in mice caused embryonic lethality[25] because intracellular acidification is crucial for many biological processes such as membrane trafficking and protein degradation in almost all cell types.[10,48] Consistently, depletion of d2 in this study (Fig. 2) abolished the extracellular acidification but the intracellular acidified compartments remained, indicated by the red fluorescence in the cytoplasm (Figs. 5A and 5B). In addition, *Atp6v0d2*$^{-/-}$ osteoclasts showed similar activities of ATP hydrolysis and proton transport to the wildtype cells, probably also resulting from the intact d1 activity because the osteoclasts were not activated in the in vitro experimental condition.[29] In support of this point, in our proton transport experiments, d2KD-day3 osteoclasts showed compromised activity compared with UT (Figs. 5J and 5N). The remaining activity should come from the contribution of intact d1. Additionally, when using the same amounts of prepared microsomes from d2KD-day1 osteoclasts, the proton-pumping activity is comparable with UT, indicating that the d1-integrated V-ATPase in intracellular compartments could complement the total V-ATPase acidification capacity in our experimental condition (Figs. 5J and 5N). Interestingly, both d1 and d2 could bind a3N1, although the interaction of a3N1 with d1 seemed weaker than with d2 (Figs. 6D and 6E), suggesting that d1 may physiologically associate with the proton pump by binding a3 in intracellular V-ATPase of osteoclasts.

Dual functions of d2 in osteoclasts

Our proposal that d2 has dual functions fits with its increasing expression profile in osteoclast differentiation. When d2 appears at an early stage (Supplementary Fig. 1A, left), it plays its regulatory role in maturation, a process of pre-osteoclast fusion.[29] However, the expression pattern could not be fully explained by d2 regulation only in osteoclast maturation. In particular, the level of d2 protein expression was even higher at day 5, a stage of post-maturation (Supplementary Fig. 1A, right) when a number of functional genes of osteoclasts have been induced, such as the *calcitonin receptor*, *cathepsin K,* and *Clc-7*.[34,49,50] This suggests that d2 may function in bone resorption in addition to cell fusion. The differentiation stage-specific depletion of d2 was thus applied for the functional analysis in osteoclast differentiation. This is a more mild and controllable approach than the global inactivation of important genes. Mono- or di-nucleated pre-osteoclasts co-exist with mature osteoclasts at day 4 (Supplementary Fig. 1B). Some MNCs, which were shown to contribute to bone resorption (Figs. 4J–4K), had already emerged on day 3 in our observation (Supplementary Fig. 1B) before the lentivirus infection in d2KD-day3 cells. Interestingly, maturation of the *Atp6v0d2*$^{-/-}$ pre-osteoclasts could be restored when mixed with some wildtype pre-osteoclasts as ''seed'' cells for fusion.[29] Thus, it could not be excluded that the normal maturation in d2KD-day3 osteoclasts was also attributed to MNCs that had emerged already before d2 depletion (Fig. 3). The d2KD-day3 osteoclasts in our experiment are similar to *Atp6v0a3*$^{-/-}$ osteoclasts[21] with the abolishment of extracellular acidification and the maintenance of V-ATPase activities in intracellular organelles (Fig. 5), adding convincing proof of the function of d2 in V-ATPase activity besides in cell fusion.

Function of d2 in cell fusion

The molecular mechanism(s) by which d2 regulates cell fusion is still unclear, although transgenic rescues with either *Adam8* or *Adam12* were shown to restore normal maturation of *Atp6v0d2*$^{-/-}$ pre-osteoclasts.[29,51,52] Because the two *Adams* have also been shown to contribute to cell fusion and osteoclastogenesis,[51,52] it remains unclear whether Adam is a downstream factor of d2. Recently, the participation of the V_0 domain and its subunits in membrane fusion independent of V-ATPase activities has been reported.[53,54] For example, *vha100-1(v100)*, the fly subunit a1, has been shown to function downstream of soluble NSF-attachment protein receptors (SNAREs) in synaptic vesicle fusion.[53] Interestingly, mouse a3 may also contribute to osteoclast fusion based on its higher expression in larger osteoclasts ($\geq$10 nuclei) than in smaller osteoclasts ($\leq$5 nuclei).[55] Therefore, d2 may participate in membrane fusion through its close association with subunits of the V_0 domain such as with a3 shown in our GST pull-down and Co-IP experiments (Fig. 6). It may also be significant to characterize the functional domains in the d2 protein that control regulation in cell fusion or in extracellular acidification.[56]

Function of subunit d2 in the extracellular acidification of V-ATPase and bone resorption

The evidences that d2 is a component of the proton pump include its interaction with a3, localization in the ruffled border, high induction by RANKL, high expression in mature osteoclasts, and the loss of extracellular acidification and bone resorption in vitro after d2 knockdown. However, the d2 knockout mouse osteopetrosis phenotype is not as severe as the a3 knockout mice.[21,29] The main discrepancy between the results from Lee et al.[29] and our own work is whether d2 is involved in bone resorption and extracellular acidification beyond cell fusion function. Actually, our data could match each other well. First, Lee et al.[29] stated that bone resorption was very low because multinucleated cells did not form. However, usually mononuclear pre-osteoclasts already have a bone resorption capability (Fig. 4K). In other words, mononuclear TRACP^{+} cells should have possessed bone resorption ability through extracellular acidification as observed in experiments in our laboratory. The impairment of bone resorption activity in the Atp6v0d2$^{-/-}$ pre-osteoclasts juts added proof that d2 deficiency may impair osteoclast function such as bone resorption and extracellular acidification.[29] Second, Lee et al.[29] reported normal V-ATPase activity in d2 mutant mice. This result is actually in accordance with our proton transport data about d2KD-day1 (Figs. 5J–5N). One possible explanation is that when d2 is absent, d1 may be able to partially replace d2 functions so that proton pumping is not completely lost. Another reason as described above is that using the same amounts of microsomes for the experiments would complement the impairment of d2 function, just as we experienced with d2KD-day1 microsomes. Third, data of d2

depletion at an early stage in our experiments matched the results from Lee et al.[29] (Fig. 3). A unique advantage of using our lentivirus-mediated RNAi knockdown is that we could also study mononuclear osteoclasts with d2 knockdown. Our in vitro RNAi study indicated that the osteopetrosis phenotype is responsible for the lack of sufficient proton pump activities caused by both the lessened MNC formation and the impairment of d2 function (Figs. 4 and 5). Therefore, our work could complement the gene targeting work because the study from Lee et al.[29] did not address the function of d2 in extracellular acidification,[29] partially because of the fact that severe impairment of the global deletion of d2 in mice precluded the possibility of studying role(s) of d2 in matured osteoclast functions. Fourth, the direct interaction between d2 and a3 adds proof for the relationship of d2 and V-ATPase (Figure 6). In accordance with this point, other reports have also shown that d2 seemed to contribute directly to V-ATPase activity because d2 could complement the vma6D phenotype in yeast caused by the deficiency of subunit d homolog and that the elevated expression of d2 could stimulate the activity of V-ATPase in XS52 dendritic cells.[15,27] Collectively, these data suggest that d2 might be functionally active in bone resorption and acidification beyond cell fusion regulation.

Relationship of d2 and other pump subunits of V-ATPase

It seems that d2 may serve as a positive regulator of acid production based on our functional analysis from d2 depletion cells (Figs. 4 and 5). Although structure studies have shown that subunit d is located in the interface of the V_0 and V_1 domains and might be essential for V_0/V_1 coupling,[11,56] the understanding of the functional significance of d2 as a component of V-ATPase depends on the elucidation of its incorporation and relationship with other pump subunits.[43] Similar expression patterns of d2 and a3 were found in osteoclast induction in vitro (data not shown), indicating their close relationship. A previous report has shown the co-localization of d2 and a3 in the plasma membrane of human osteoclasts.[26] This was consistent with our Co-IP results that showed the association between mouse d2 and a3 when overexpressed in HEK-293T cells (Fig. 6B). This was further supported when we first reported that d2 could directly interact with the N terminus of a3 (a3N1, aa 1–387 of full-length a3 using GST pull-down assay; Fig. 6E, left). Interestingly, we could not observe the interaction between d2 and the N-terminal a3N2 (aa 1–178), indicating that the binding between d2 and a3 may happen in the aa region of 179–387 in a3 (Fig. 6E, right), which still needs to be further characterized. Consistently, a3 and d2 could co-localize in the lysosomes of NIH-3T3 cells (Supplementary Fig. 3). A recent study of the yeast homolog of subunit a showed that it has a role in the dissociation of V_1 and V_0 , whereas the C-terminal nine transmembrane domain was shown to be critical to V_1/V_0 coupling efficiency.[45] The interaction between d2 and a3N1 showed that d2 might function in targeting and in vivo dissociation through binding with subunit a3 on the activation of osteoclasts. However, because of the lack of good antibodies for Co-IP experiments, further confirmation of the endogenous association between d2 and a3 still needs to be studied. The assumption that osteoclast V-ATPases in the plasma membrane select a different combination of subunits or isoforms from the intracellular proton pump including the subunits a3, B2, C1, and d2, may be elucidated when more evidence of interaction emerge among those osteoclast-specific components.

In summary, this study suggests the dual functions of d2 in osteoclasts, especially for extracellular acidification, and it adds d2 to the list of subunits identified as components of the osteoclast-specific V-ATPase in the plasma membrane. Although additional experiments are needed to elucidate the molecular mechanisms by which d2 functions in osteoclasts, our findings point to d2 as a potential therapeutic target for the treatment of human diseases caused by excessive activity of osteoclasts, such as osteoporosis and rheumatoid arthritis.[4–6]

ACKNOWLEDGMENTS

We thank Christie Taylor and Carrie Soltanoff for manuscript assistance; Dr. Shengmei Feng and Dr. Wei Chen for critical discussion and technical assistance of this work; Dr. Jiuhong Kang (Institute of Biochemistry and Cell Biology, Chinese Academy of Science, Shanghai, China) for kindly providing the lentivirus vector and packaging plasmids; Yihui Tu for assistance of confocal microscopy; and Jiqin Li for SEM assistance. Work in G-L.X.'s laboratory is supported by grants from the China National Science Foundation, the Ministry of Science and Technology of China (National Basic Research Program 2005CB522400), the Shanghai Municipal Commission for Science and Technology, and the Max-Planck-Gesellschaft zur Forderung der Wissenschaften (the Max Planck Society for the Advancement of Science). The work in Y-P.L.'s laboratory is supported by NIH Grant AR-44741.

REFERENCES

1. Teitelbaum SL 2000 Bone resorption by osteoclasts. Science **289:**1504–1508.
2. Boyle WJ, Simonet WS, Lacey DL 2003 Osteoclast differentiation and activation. Nature **423:**337–342.
3. Teitelbaum SL, Ross FP 2003 Genetic regulation of osteoclast development and function. Nat Rev Genet **4:**638–649.
4. Rodan GA, Martin TJ 2000 Therapeutic approaches to bone diseases. Science **289:**1508–1514.
5. Zelzer E, Olsen BR 2003 The genetic basis for skeletal diseases. Nature **423:**343–348.
6. Tolar J, Teitelbaum SL, Orchard PJ 2004 Osteopetrosis. N Engl J Med **351:**2839–2849.
7. Zhao Q, Shao J, Chen W, Li YP 2007 Osteoclast differentiation and gene regulation. Front Biosci **12:**2519–2529.
8. Vaananen HK, Zhao H, Mulari M, Halleen JM 2000 The cell biology of osteoclast function. J Cell Sci **113:**377–381.
9. Blair HC, Teitelbaum SL, Ghiselli R, Gluck S 1989 Osteoclastic bone resorption by a polarized vacuolar proton pump. Science **245:**855–857.
10. Nishi T, Forgac M 2002 The vacuolar (H+)-ATPases–nature's most versatile proton pumps. Nat Rev Mol Cell Biol **3:**94–103.

11. Forgac M 2007 Vacuolar ATPases: rotary proton pumps in physiology and pathophysiology. Nat Rev Mol Cell Biol **8:**917–929.
12. Baron R, Neff L, Louvard D, Courtoy PJ 1985 Cell-mediated extracellular acidification and bone resorption: evidence for a low pH in resorbing lacunae and localization of a 100-kD lysosomal membrane protein at the osteoclast ruffled border. J Cell Biol **101:**2210–2222.
13. Recchi C, Chavrier P 2006 V-ATPase: a potential pH sensor. Nat Cell Biol **8:**107–109.
14. Smith AN, Lovering RC, Futai M, Takeda J, Brown D, Karet FE 2003 Revised nomenclature for mammalian vacuolar-type H+-ATPase subunit genes. Mol Cell **12:**801–803.
15. Nishi T, Kawasaki-Nishi S, Forgac M 2003 Expression and function of the mouse V-ATPase d subunit isoforms. J Biol Chem **278:**46396–46402.
16. Smith AN, Borthwick KJ, Karet FE 2002 Molecular cloning and characterization of novel tissue-specific isoforms of the human vacuolar H(+)-ATPase C, G and d subunits, and their evaluation in autosomal recessive distal renal tubular acidosis. Gene **297:**169–177.
17. Sun-Wada GH, Yoshimizu T, Imai-Senga Y, Wada Y, Futai M 2003 Diversity of mouse proton-translocating ATPase: presence of multiple isoforms of the C, d and G subunits. Gene **302:**147–153.
18. Sun-Wada GH, Imai-Senga Y, Yamamoto A, Murata Y, Hirata T, Wada Y, Futai M 2002 A proton pump ATPase with testis-specific E1-subunit isoform required for acrosome acidification. J Biol Chem **277:**18098–18105.
19. Li YP, Chen W, Stashenko P 1996 Molecular cloning and characterization of a putative novel human osteoclast-specific 116-kDa vacuolar proton pump subunit. Biochem Biophys Res Commun **218:**813–821.
20. Deng W, Stashenko P, Chen W, Liang Y, Shimizu K, Li YP 2001 Characterization of mouse Atp6i gene, the gene promoter, and the gene expression. J Bone Miner Res **16:**1136–1146.
21. Li YP, Chen W, Liang Y, Li E, Stashenko P 1999 Atp6i-deficient mice exhibit severe osteopetrosis due to loss of osteoclast-mediated extracellular acidification. Nat Genet **23:**447–451.
22. Frattini A, Orchard PJ, Sobacchi C, Giliani S, Abinun M, Mattsson JP, Keeling DJ, Andersson AK, Wallbrandt P, Zecca L, Notarangelo LD, Vezzoni P, Villa A 2000 Defects in TCIRG1 subunit of the vacuolar proton pump are responsible for a subset of human autosomal recessive osteopetrosis. Nat Genet **25:**343–346.
23. Feng S, Deng L, Chen W, Shao J, Xu G, Li YP 2008 Atp6v1c1 is an essential component of the osteoclast proton pump and in F-actin ring formation in osteoclasts. Biochem J **417:**195–203.
24. Norgett EE, Borthwick KJ, Al-Lamki RS, Su Y, Smith AN, Karet FE 2007 V1 and V0 domains of the human H+-ATPase are linked by an interaction between the G and a subunits. J Biol Chem **282:**14421–14427.
25. Miura GI, Froelick GJ, Marsh DJ, Stark KL, Palmiter RD 2003 The d subunit of the vacuolar ATPase (Atp6d) is essential for embryonic development. Transgenic Res **12:**131–133.
26. Smith AN, Jouret F, Bord S, Borthwick KJ, Al-Lamki RS, Wagner CA, Ireland DC, Cormier-Daire V, Frattini A, Villa A, Kornak U, Devuyst O, Karet FE 2005 Vacuolar H+-ATPase d2 subunit: molecular characterization, developmental regulation, and localization to specialized proton pumps in kidney and bone. J Am Soc Nephrol **16:**1245–1256.
27. Sato K, Shikano S, Xia G, Takao J, Chung JS, Cruz PD Jr, Xie XS, Ariizumi K 2006 Selective expression of vacuolar H+-ATPase subunit d2 by particular subsets of dendritic cells among leukocytes. Mol Immunol **43:**1443–1453.
28. Pietrement C, Sun-Wada GH, Silva ND, McKee M, Marshansky V, Brown D, Futai M, Breton S 2006 Distinct expression patterns of different subunit isoforms of the V-ATPase in the rat epididymis. Biol Reprod **74:**185–194.
29. Lee SH, Rho J, Jeong D, Sul JY, Kim T, Kim N, Kang JS, Miyamoto T, Suda T, Lee SK, Pignolo RJ, Koczon-Jaremko B, Lorenzo J, Choi Y 2006 v-ATPase V0 subunit d2-deficient mice exhibit impaired osteoclast fusion and increased bone formation. Nat Med **12:**1403–1409.
30. Yang S, Chen W, Stashenko P, Li YP 2007 Specificity of RGS10A as a key component in the RANKL signaling mechanism for osteoclast differentiation. J Cell Sci **120:**3362–3371.
31. Yang S, Li YP 2007 RGS12 is essential for RANKL-evoked signaling for terminal differentiation of osteoclasts in vitro. J Bone Miner Res **22:**45–54.
32. Yang S, Li YP 2007 RGS10-null mutation impairs osteoclast differentiation resulting from the loss of [Ca2+]i oscillation regulation. Genes Dev **21:**1803–1816.
33. Chen W, Li YP 1998 Generation of mouse osteoclastogenic cell lines immortalized with SV40 large T antigen. J Bone Miner Res **13:**1112–1123.
34. Cappellen D, Luong-Nguyen NH, Bongiovanni S, Grenet O, Wanke C, Susa M 2002 Transcriptional program of mouse osteoclast differentiation governed by the macrophage colony-stimulating factor and the ligand for the receptor activator of NFkappa B. J Biol Chem **277:**21971–21982.
35. Ge YZ, Pu MT, Gowher H, Wu HP, Ding JP, Jeltsch A, Xu GL 2004 Chromatin targeting of de novo DNA methyltransferases by the PWWP domain. J Biol Chem **279:**25447–25454.
36. Li B, Zhou J, Liu P, Hu J, Jin H, Shimono Y, Takahashi M, Xu G 2007 Polycomb protein Cbx4 promotes SUMO modification of de novo DNA methyltransferase Dnmt3a. Biochem J **405:**369–378.
37. Xie ZH, Huang YN, Chen ZX, Riggs AD, Ding JP, Gowher H, Jeltsch A, Sasaki H, Hata K, Xu GL 2006 Mutations in DNA methyltransferase DNMT3B in ICF syndrome affect its regulation by DNMT3L. Hum Mol Genet **15:**1375–1385.
38. Bai S, Kopan R, Zou W, Hilton MJ, Ong CT, Long F, Ross FP, Teitelbaum SL 2008 NOTCH1 Regulates Osteoclastogenesis Directly in Osteoclast Precursors and Indirectly via Osteoblast Lineage Cells. J Biol Chem **283:**6509–6518.
39. David P, Baron R 1994 The catalytic cycle of the vacuolar H(+)-ATPase. Comparison of proton transport in kidney- and osteoclast-derived vesicles. J Biol Chem **269:**30158–30163.
40. Li YQ, Zhou PZ, Zheng XD, Walsh CP, Xu GL 2007 Association of Dnmt3a and thymine DNA glycosylase links DNA methylation with base-excision repair. Nucleic Acids Res **35:**390–400.
41. Chu K, Cornetta KG, Econs MJ 2008 Efficient and stable gene expression into human osteoclasts using an HIV-1-based lentiviral vector. DNA Cell Biol **27:**315–320.
42. Hu Y, Nyman J, Muhonen P, Vaananen HK, Laitala-Leinonen T 2005 Inhibition of the osteoclast V-ATPase by small interfering RNAs. FEBS Lett **579:**4937–4942.
43. Sun-Wada GH, Murata Y, Namba M, Yamamoto A, Wada Y, Futai M 2003 Mouse proton pump ATPase C subunit isoforms (C2-a and C2-b) specifically expressed in kidney and lung. J Biol Chem **278:**44843–44851.
44. Leng XH, Nishi T, Forgac M 1999 Transmembrane topography of the 100-kDa a subunit (Vph1p) of the yeast vacuolar proton-translocating ATPase. J Biol Chem **274:**14655–14661.
45. Kawasaki-Nishi S, Bowers K, Nishi T, Forgac M, Stevens TH 2001 The amino-terminal domain of the vacuolar proton-translocating ATPase a subunit controls targeting and in vivo dissociation, and the carboxyl-terminal domain affects coupling of proton transport and ATP hydrolysis. J Biol Chem **276:**47411–47420.
46. Toyomura T, Murata Y, Yamamoto A, Oka T, Sun-Wada GH, Wada Y, Futai M 2003 From lysosomes to the plasma membrane: localization of vacuolar-type H+ -ATPase with the a3 isoform during osteoclast differentiation. J Biol Chem **278:**22023–22030.
47. Kim K, Lee SH, Ha Kim J, Choi Y, Kim N 2008 NFATc1 Induces Osteoclast Fusion Via Up-Regulation of Atp6v0d2 and the Dendritic Cell-Specific Transmembrane Protein (DC-STAMP). Mol Endocrinol **22:**176–185.

48. Forgac M 1999 Structure and properties of the vacuolar (H+)-ATPases. J Biol Chem **274:**12951–12954.
49. Lange PF, Wartosch L, Jentsch TJ, Fuhrmann JC 2006 ClC-7 requires Ostm1 as a beta-subunit to support bone resorption and lysosomal function. Nature **440:**220–223.
50. Kasper D, Planells-Cases R, Fuhrmann JC, Scheel O, Zeitz O, Ruether K, Schmitt A, Poet M, Steinfeld R, Schweizer M, Kornak U, Jentsch TJ 2005 Loss of the chloride channel ClC-7 leads to lysosomal storage disease and neurodegeneration. EMBO J **24:**1079–1091.
51. Abe E, Mocharla H, Yamate T, Taguchi Y, Manolagas SC 1999 Meltrin-alpha, a fusion protein involved in multinucleated giant cell and osteoclast formation. Calcif Tissue Int **64:**508–515.
52. Choi SJ, Han JH, Roodman GD 2001 ADAM8: a novel osteoclast stimulating factor. J Bone Miner Res **16:**814–822.
53. Hiesinger PR, Fayyazuddin A, Mehta SQ, Rosenmund T, Schulze KL, Zhai RG, Verstreken P, Cao Y, Zhou Y, Kunz J, Bellen HJ 2005 The v-ATPase V0 subunit a1 is required for a late step in synaptic vesicle exocytosis in Drosophila. Cell **121:**607–620.
54. Hurtado-Lorenzo A, Skinner M, El Annan J, Futai M, Sun-Wada GH, Bourgoin S, Casanova J, Wildeman A, Bechoua S, Ausiello DA, Brown D, Marshansky V 2006 V-ATPase interacts with ARNO and Arf6 in early endosomes and regulates the protein degradative pathway. Nat Cell Biol **8:**124–136.
55. Manolson MF, Yu H, Chen W, Yao Y, Li K, Lees RL, Heersche JN 2003 The a3 isoform of the 100-kDa V-ATPase subunit is highly but differentially expressed in large (>or=10 nuclei) and small (<or= nuclei) osteoclasts. J Biol Chem **278:**49271–49278.
56. Owegi MA, Pappas DL, Finch MW Jr, Bilbo SA, Resendiz CA, Jacquemin LJ, Warrier A, Trombley JD, McCulloch KM, Margalef KL, Mertz MJ, Storms JM, Damin CA, Parra KJ 2006 Identification of a domain in the V0 subunit d that is critical for coupling of the yeast vacuolar proton-translocating ATPase. J Biol Chem **281:**30001–30014.

Received in original form May 30, 2008; revised form October 8, 2008; accepted December 22, 2008.